Intravoxel incoherent motion analysis of abdominal organs: application of simultaneous multislice acquisition

Phi Van, Valerie Doan ; Becker, Anton S ; Ciritsis, Alexander ; Reiner, Caecilia S ; Boss, Andreas

Abstract: PURPOSE: The aim of this study was to systematically evaluate the accuracy of quantitative intravoxel incoherent motion (IVIM) analysis of the upper abdomen applying simultaneous multislice (SMS) diffusion-weighted imaging (DWI) to reduce acquisition time. MATERIALS AND METHODS: Diffusion-weighted imaging of parenchymal abdominal organs was performed in 8 healthy volunteers at 3 T using a standard DWI sequence (acceleration factor 1 [AF1]) and an SMS-accelerated echo planar imaging sequence with acceleration factors 2 and 3 (AF2/AF3). Intravoxel incoherent motion analysis was performed with a multistep algorithm for true diffusion coefficient (Dt), pseudodiffusion coefficient (D*), and fraction of perfusion (Fp) measured for the liver, kidney cortex and medulla, pancreas, spleen, and erector spinae muscle. Qualitative and quantitative parameters were compared using a repeated measurement 1-way analysis of variance test and the Bonferroni post hoc method. RESULTS: Simultaneous multislice DWI provided diagnostic image quality in all volunteers with a reduction of scan time of 50% for AF2 (67% for AF3) compared with the standard sequence. Decent IVIM analysis for Dt, D*, and Fp can be calculated on the images of both the SMS sequences AF2 and AF3 with typical organ characteristics of IVIM; however, systematical deviations from AF1 were observed: Dt values increased and Fp decreased significantly with higher acceleration factor for liver, kidney, pancreas, and muscle ($P < 0.05$). Fitting curves of higher acceleration factors tend to be more monoexponentially shaped. CONCLUSIONS: Simultaneous multislice acceleration provides considerable scan time reduction for upper abdomen DWI with equivalent quality of IVIM analysis compared with the standard nonaccelerated technique. Systematic discrepancies of the true Dt, D*, and Fp for SMS acquisitions need to be considered when comparing to standard DWI sequences.

DOI: https://doi.org/10.1097/RLI.0000000000000426

Intravoxel Incoherent Motion Analysis of Abdominal Organs
Application of Simultaneous Multislice Acquisition

Valerie Doan Phi Van, MD, Anton S. Becker, MD, Alexander Ciritsis, PhD, Caecilia S. Reiner, MD, and Andreas Boss, MD, PhD

Purpose: The aim of this study was to systematically evaluate the accuracy of quantitative intravoxel incoherent motion (IVIM) analysis of the upper abdomen applying simultaneous multislice (SMS) diffusion-weighted imaging (DWI) to reduce acquisition time.

Materials and Methods: Diffusion-weighted imaging of parenchymal abdominal organs was performed in 8 healthy volunteers at 3 T using a standard DWI sequence (acceleration factor 1 [AF1]) and an SMS-accelerated echo planar imaging sequence with acceleration factors 2 and 3 (AF2/AF3). Intravoxel incoherent motion analysis was performed with a multistep algorithm for true diffusion coefficient (D_t), pseudodiffusion coefficient (D^*), and fraction of perfusion (F_p) measured for the liver, kidney cortex and medulla, pancreas, spleen, and erector spinae muscle. Qualitative and quantitative parameters were compared using a repeated measurement 1-way analysis of variance test and the Bonferroni post hoc method.

Results: Simultaneous multislice DWI provided diagnostic image quality in all volunteers with a reduction of scan time of 50% for AF2 (67% for AF3) compared with the standard sequence. Decent IVIM analysis for D_t, D^*, and F_p can be calculated on the images of both the SMS sequences AF2 and AF3 with typical organ characteristics of IVIM; however, systematical deviations from AF1 were observed: D_t values increased and F_p decreased significantly with higher acceleration factor for liver, kidney, pancreas, and muscle ($P < 0.05$). Fitting curves of higher acceleration factors tend to be more monoexponentially shaped.

Conclusions: Simultaneous multislice acceleration provides considerable scan time reduction for upper abdomen DWI with equivalent quality of IVIM analysis compared with the standard nonaccelerated technique. Systematic discrepancies of the true D_t, D^*, and F_p for SMS acquisitions need to be considered when comparing to standard DWI sequences.

Key Words: intravoxel incoherent motion, simultaneous multislice acquisition, abdominal organs, diffusion imaging

(*Invest Radiol* 2017;00: 00–00)

With the latest advances in diffusion-weighted imaging (DWI), magnetic resonance imaging (MRI) plays an increasingly important role in clinical routine.[1] Diffusion-weighted imaging is an imaging technique based on characterizing different tissues by measuring the degree of water free motion because the molecular movement of water reflects its interaction with the microarchitecture of the tissue.[2] Diffusion-weighted imaging was firstly applied to the central nervous system with the most common indication being the detection of acute stroke.[3] With the improvement of gradient coil design and parallel imaging read-out techniques, DWI can now also be applied to a wide range of the abdominal organs with excellent imaging quality.[4]

In abdominal organs, DWI has been shown to be useful for the detection and differential diagnosis of focal lesions of the liver,[5] kidney,[6] pancreas,[7] prostate,[8] and uterus.[9] Diffusion-weighted imaging in oncological imaging is based on the higher cellularity of cancer tissue in comparison to healthy neighboring tissue and consequently the higher diffusion restriction of water movement by cellular membranes.[10] It has also been shown that DWI is capable to characterize and stage liver fibrosis with increasing diffusion restriction for more severe stages.[11]

In DWI, the degree of water diffusion in tissue is quantified by the apparent diffusion coefficient. A monoexponential mathematical model is applied to calculate the apparent diffusion coefficient from the signal decay observed at different b-values. Although the model is quite successful in clinical routine, it ignores the influence of capillary microperfusion of the tissue, which contributes to the measured MRI signal at low b-values. Suggested by Le Bihan et al,[12] microperfusion can be described as a second exponential component in an intravoxel incoherent motion (IVIM) model. In contrast to the standard monoexponential model, the IVIM model for analysis of DWI data sets, including both multiple high and low b-values, offers a mathematical model to distinguish the diffusion signal of passive water diffusion (true diffusion) and the perfusion-related diffusion component (pseudodiffusion) originating from capillary microperfusion.

Using an IVIM analysis with calculation of biomarkers for both free passive water movement and microperfusion allows a more comprehensive characterization of tissues. Intravoxel incoherent motion analysis was shown to be useful for the discrimination between benign and malignant liver lesions.[13] Furthermore, it was demonstrated that IVIM analysis is able to improve the characterization of hepatocellular carcinoma compared with conventional DWI.[14] Further studies showed the capability of the IVIM model to predict therapy response in the treatment of malignant lesions, such as antiangiogenetic chemotherapy or radiofrequency ablation in animal models and in clinical studies.[15,16]

Nevertheless, there are 2 major challenges with the clinical application of IVIM analysis. First, DWI is a technique with an intrinsically low signal yield requiring many repetitions and subsequently long acquisition time (TA).[17] Second, IVIM analysis relies on the acquisition of many more b-values compared with the standard monoexponential DWI model resulting in even longer examination times, which severely hampers the applicability of IVIM in clinical routine MRI protocols.

Recent advances in simultaneous multislice (SMS) imaging seem an option to drastically reduce the scan time by an acceleration factor (AF) of 2 or 3. The underlying technique is based on the excitation of multiple slices simultaneously and the subsequent antialiasing to reconstruct the magnitude images. Simultaneous multislice sequences have successfully been tested for DWI of the human brain,[18] the breast,[19] the prostate,[20] the liver, the pancreas,[21] and the kidneys.[22] However, the SMS technique shows some limitations regarding image quality and signal-to-noise ratio due to aliasing problems between the simultaneous excited neighboring slices, which may affect diffusion measurements and IVIM analysis.[19,23]

Received for publication July 4, 2017; and accepted for publication, after revision, September 14, 2017.

From the Institute of Diagnostic and Interventional Radiology, University Hospital Zurich, Zurich, Switzerland.

Correspondence to: Valerie Doan Phi Van, MD, Institute of Diagnostic and Interventional Radiology, University Hospital Zurich, Rämistr. 100 8091 Zurich, Switzerland. E-mail: ValerieDoan.PhiVan@usz.ch.

ISSN: 0020-9996/17/0000–0000
DOI: 10.1097/RLI.0000000000000426

We hypothesize that IVIM calculations based on SMS-DWI sequences can yield very similar results to standard DWI sequences. In the present investigation, we systematically address the accuracy of SMS-DWI sequences in the application to IVIM measurements of parenchymal organs of the upper abdomen and to determine the optimal acceleration factor.

MATERIALS AND METHODS

Subjects

A prospective study was carried out including 8 healthy volunteers (3 men and 5 women; mean age, 28 years; range, 24–35 years), which was approved by the local ethics committee. Written informed consent was obtained from all volunteers. None of the volunteers experienced any discomfort during the examination.

Magnetic Resonance Imaging

All scans were performed in a 3 T MRI scanner (Skyra Siemens Healthcare, Erlangen, Germany, with Siemens software version syngo MR E 11) using a flexible 18-channel matrix coil and the built-in 32-channel spine coil. After the localizer, the protocol consisted of the standard DWI echo planar imaging sequence (AF1) and a single-shot spin-echo echo planar imaging DWI sequence (WIP prototype sequence) capable of SMS with blipped controlled aliasing in parallel imaging results in higher acceleration readout. Two SMS-DWI sequence acquisitions were performed with an AF2 and AF3. For IVIM analysis, 10 different b-values (0, 10, 30, 60, 120, 200, 300, 430, 600, 800 s/mm^2) were acquired with averages 1/2/2/2/2/2/3/4/6/8. The TA in the accelerated sequences could be reduced due to a possible reduction in the repetition time (TR):

Sequence A: AF1 (TR, 6900 milliseconds; TA, 11:44 minutes).
Sequence B: AF2 (TR, 3500 milliseconds; TA, 6:06 minutes)
Sequence C: AF3 (TR, 2400 milliseconds; TA, 4:17 minutes).

Further parameters of the sequence were echo-time of 65 milliseconds; number of slices, 42; slice thickness, 5 mm; field of view, 400 mm; field of view phase, 78.1%; in-plane resolution, 2.1 × 2.1 mm^2; pixel bandwidth, 1736 px/Hz; and diffusion mode: 3-scan trace, parallel imaging generalized autocalibrating partial parallel acquisition (factor 2), spectral attenuated inversion recovery fat-suppression. Examinations were performed under shallow breathing.

Postprocessing by Region of Interest Evaluation

A polygonal region of interest (ROI) with typical ROI size of 50 to 900 mm^2 was placed into the right liver in segment VI and the left liver lobe in segment IVa/b, the right/left renal cortex and medulla on the height of the hilum, the pancreatic tail, the middle of the spleen, and the erector spinae muscle on the left side. At first, the ROI was drawn on the images of b = 0 s/mm^2 and subsequently copied to the corresponding images at higher b-values. Typical ROI definitions are depicted in Figure 1. The ROI was first placed in the data set of the standard sequence and then automatically copied onto the data set of AF2 and AF3 to avoid differences due to manual placement.

IVIM Analysis

Postprocessing of DWI data sets was performed using an in-house routine implemented in Matlab (The MathWorks, Natick, MA). In the IVIM analysis, the signal intensity curves from DWI measurements with multiple b-values are described by the following biexponential model:

$$S_b/S_0 = \left(1-F_p\right)\exp(-bD_t) + F_p\exp(-bD) \qquad 1$$

with S_b corresponding to the signal intensity in the DWI data set acquired with the b-value b, S_0 to the signal intensity at b = 0 s/mm^2, F_p to the perfusion fraction, D^* to the pseudodiffusion of the perfusion compartment, and D_t to the "true" diffusion coefficient of passive molecular water diffusion. A multistep algorithm was applied to obtain stable IVIM parameters as previously described.[23] In short, the first step D_t is calculated from the log transformed signal intensities of the larger b-values. The b-value threshold is dynamically chosen with smallest residuals of the later biexponential fit. In a second step, F_p is determined from the signal intensity of the b0-measurement and the y axis intercept

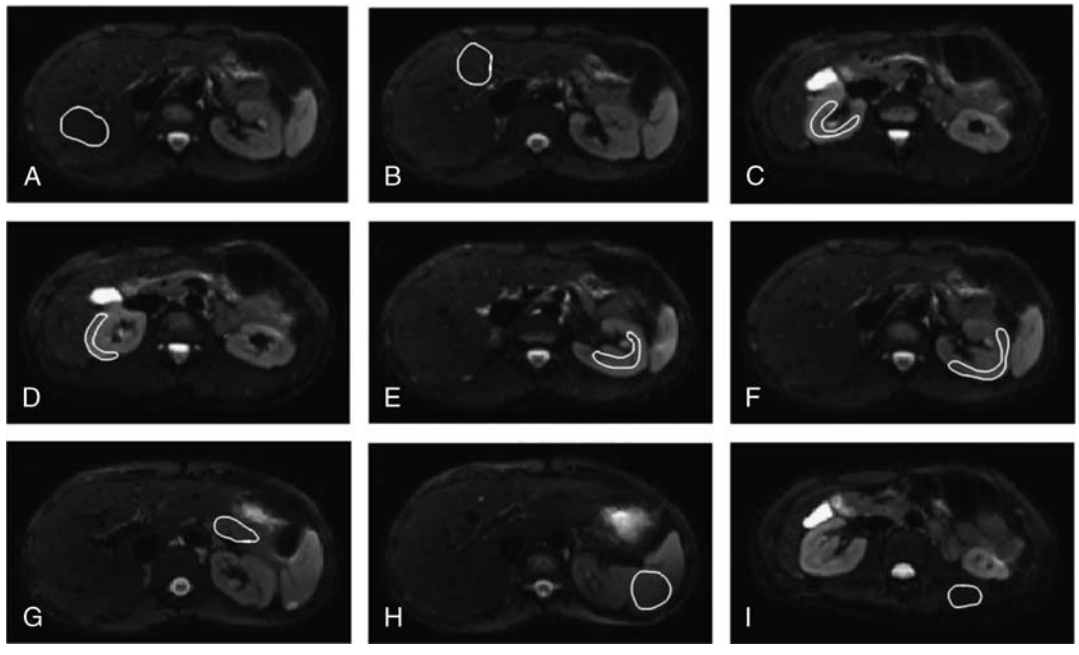

FIGURE 1. Example of selected ROIs in the right/left liver lobe, kidney cortex and medulla, pancreas, spleen, and left erector spinae muscle for IVIM analysis.

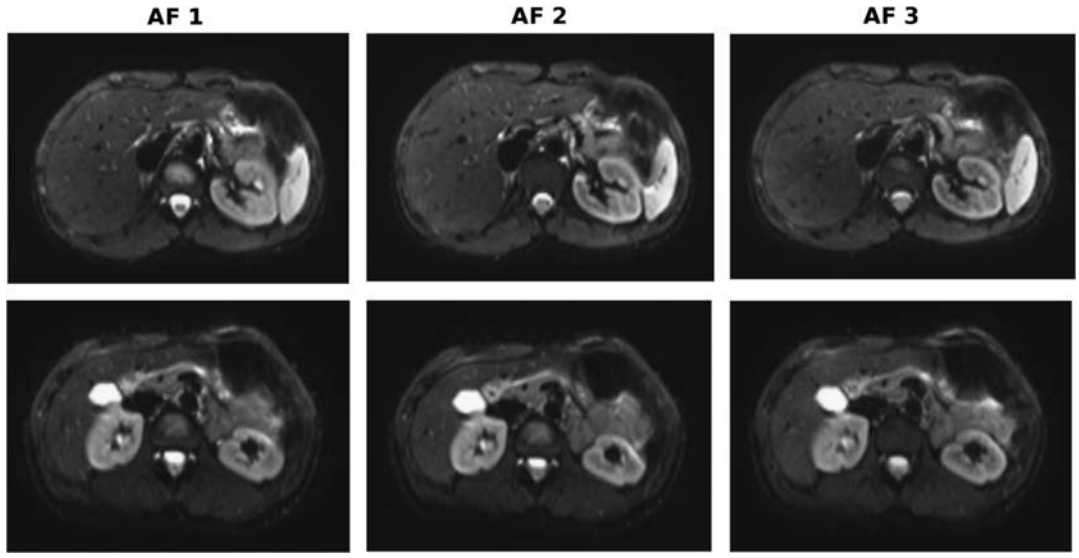

FIGURE 2. Example of 2 slices for the 3 different sequences (standard, AF2, and AF3). Sustained image quality in AF1 and AF2 with slight loss of image quality in AF3.

of the previous polygonal fit of the first step. These 2 parameters are held constant in the consecutively calculated D^* value using a full biexponential nonlinear fit.

Statistical Analysis

Statistical analysis was performed using the statistics program GraphPad Prism 7 (GraphPad Software Inc, San Diego, CA). For descriptive analysis, mean values and standard deviations were calculated for each organ and each sequence (AF1–AF3). Values for liver, kidney cortex, and kidney medulla were calculated as mean values of both sides. F-test was performed to show the significant difference in standard deviation between the IVIM parameters. One-way analysis of variance was applied to test for differences in the mean values of the true diffusion coefficient (D_t), perfusion fraction (F_p), and pseudodiffusion coefficient (D^*) between different acceleration factors. Bonferroni post hoc correction was performed for multiple comparisons. GraphPad Prism was used to depict the results in box plots and Bland-Altman plots.

RESULTS

Qualitative Assessment of the Image Quality

All data sets were successfully acquired with complete depiction of all parenchymal abdominal organs. None of the examinations had to be excluded due to breathing artifacts hampering the evaluation and the ROI analysis. No artifacts due to problems with fat saturation were observed. No pathological findings were detected in the organs of the upper abdomen of all study objects. Image quality of both the standard nonaccelerated sequence (AF1) and the sequence with AF2 were

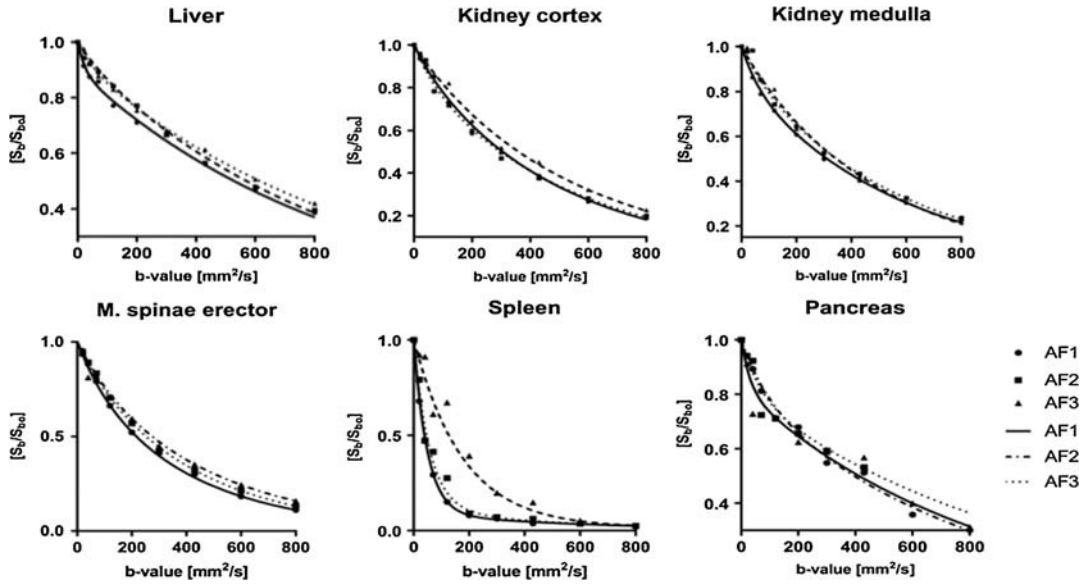

FIGURE 3. Typical biexponential fitting curves of liver, kidney, spleen, pancreas, and muscle tissue for AF1, AF2, and AF3. Note the loss of the biexponential character in the fitting curve of AF2 and AF3 in comparison to AF1 for low b-values up to 200 mm^2/s.

comparable, whereas quality was visibly decreased applying an AF3 (Fig. 2). The typical IVIM behavior was seen in the signal curves with fast signal decay for low b-values in liver and spleen, and more gradual signal decay for the other organs (kidney, muscle). Example signal decay curves (with corresponding IVIM fits) are depicted in Figure 3.

Quantitative IVIM Parameters of the Nonaccelerated Sequence (AF1)

The true diffusion coefficient D_t, the perfusion fraction F_p, and the pseudodiffusion D^* are provided in Table 1 (first line in each row) for all parenchymal abdominal organs. The highest true diffusion value D_t was measured in the kidneys (cortex, $1.58 \pm 0.17 \times 10^{-3}$ mm^2/s; medulla, $1.52 \pm 0.16 \times 10^{-3}$ mm^2/s) and slightly lower in the pancreas ($1.14 \pm 0.21 \times 10^{-3}$ mm^2/s) and muscle ($1.38 \pm 0.20 \times 10^{-3}$ mm^2/s), whereas the liver ($0.88 \pm 0.04 \times 10^{-3}$ mm^2/s) and the spleen ($0.74 \pm 0.29 \times 10^{-3}$ mm^2/s) exhibited lowest D_t values. Regarding the perfusion-dependent parameter "pseudodiffusion" D^*, the highest D^* values were obtained in the liver ($56.25 \pm 23.88 \times 10^{-3}$ mm^2/s) and the spleen ($33.94 \pm 26.43 \times 10^{-3}$ mm^2/s). Kidney (cortex, $14.86 \pm 14.42 \times 10^{-3}$ mm^2/s; medulla, $16.56 \pm 15.99 \times 10^{-3}$ mm^2/s) and pancreas ($12.03 \pm 9.15 \times 10^{-3}$ mm^2/s) both showed lower D^* values with the lowest D^* for muscle ($8.07 \pm 3.06 \times 10^{-3}$ mm^2/s). The values of the perfusion fraction F_p were very similar for liver (0.26 ± 0.29) and kidney (cortex, 0.26 ± 0.06; medulla, 0.28 ± 0.10), slightly higher for pancreas (0.36 ± 0.09), and lower for muscle (0.13 ± 0.03) and the spleen (0.08 ± 0.04). F-test demonstrated that the standard deviation of the D^* values are higher in comparison with D_t and F_p values, especially for the spleen ($P < 0.0001$) and the pancreas ($P < 0.0001$).

Characteristics of IVIM Parameters in AF2 and AF3

The characteristic combination of IVIM parameters D_t, F_p, and D^* was preserved in accelerated sequences for all abdominal organs (Fig. 4, Table 1) with highest values for D_t detected in the kidneys and lowest values for D_t found in liver and spleen. Consecutively, highest values for pseudodiffusion D^* were measured in the liver and lowest value for D^* in the muscle tissue. Similarly, perfusion fraction F_p was measured highest in the liver and kidney, and lowest in the spleen.

Quantitative Differences Between the Standard Sequence (AF1) and Accelerated Sequences (AF2 and AF3)

Higher acceleration factor resulted in typical deviations in the D_t and F_p values compared with AF1. All measured values are listed in Table 1 for each acceleration factor. D_t systematically increases with higher acceleration factor in all tissues from AF1 to AF3 ($P < 0.05$). The increase of D_t is a typical pattern found in all abdominal organs (Fig. 5) as can be seen from Bland-Altman plots in Figure 6 with the most obvious systematic dependency on the acceleration factor in the liver. Similarly, the perfusion fraction F_p slightly decreases with higher acceleration factor for all organs (P value < 0.05, Fig. 5). No clear trend was discovered for D^*. In Table 2, conversion factors are displayed to convert the IVIM parameters D_t and F_p between different acceleration factors.

In summary, 2 main findings were observed: (1) higher D_t and lower F_p values with accelerated sequences; and (2) a slight loss of the biexponential curve shape with main characteristics of individual abdominal organs being preserved at AF2 and AF3 (Table 3).

DISCUSSION

In our study, IVIM analysis based on SMS-DWI was compared with the standard nonaccelerated DWI sequence. We could show that IVIM analysis based on SMS-DWI sequences with moderate acceleration factors AF2 and AF3 yields comparable values for D_t, F_p, and D^* to those obtained from standard DWI sequences. Applying SMS sequences, a substantial scan time reduction of 50% with AF2 and 67% with AF3 can be reached, thereby rendering IVIM acquisitions compatible with clinical constraints. As slight systematic deviations of IVIM parameters occur between different acceleration factors, only parameters of identical acceleration factors should be compared or parameters need to be converted by the appropriate conversion factor.

Our results show that IVIM analysis based on SMS-DWI sequences results in 2 systematical deviations compared with the standard sequence. First, the D_t coefficients calculated from the SMS-DWI images are systematically higher compared with the standard sequence, while the fraction of perfusion (F_p) decreases with the higher acceleration factor. This deviation becomes more prominent with higher acceleration factors. A reason for the lower F_p value may be found in the interdependence of F_p and D_t in the IVIM parameter calculation. As D_t is calculated first in the multistep approach, a higher D_t

TABLE 1. Mean ± SD of the Measured IVIM Parameters D_t, F_p, and D^* for Upper Abdominal Organs and Skeletal Muscle and for AF1 to AF3

	Liver	Kidney Cortex	Kidney Medulla	Pancreas	Spleen	Erector Spinae Muscle
D_t, mm^2/s						
AF1	0.88 ± 0.04	1.58 ± 0.17	1.52 ± 0.16	1.14 ± 0.21	0.74 ± 0.29	1.38 ± 0.20
AF2	0.95 ± 0.10*	1.65 ± 0.18*	1.64 ± 0.20*	1.30 ± 0.20	0.94 ± 0.27	1.60 ± 0.09*
AF3	1.19 ± 0.14*	1.83 ± 0.18*	1.80 ± 0.22*	1.54 ± 0.34*	1.29 ± 0.30*	1.70 ± 0.16*
F_p						
AF1	0.26 ± 0.29	0.26 ± 0.06	0.28 ± 0.10	0.36 ± 0.09	0.09 ± 0.17	0.13 ± 0.03
AF2	0.21 ± 0.23*	0.18 ± 0.05*	0.20 ± 0.05*	0.24 ± 0.09*	0.08 ± 0.09	0.11 ± 0.10*
AF3	0.15 ± 0.22*	0.15 ± 0.05*	0.12 ± 0.60*	0.22 ± 0.11	0.01 ± 0.03*	0.08 ± 0.05*
D^*, mm^2/s						
AF1	56.52 ± 23.88	14.86 ± 14.42	16.56 ± 15.99	12.03 ± 9.15	33.94 ± 26.43	8.07 ± 3.06
AF2	49.74 ± 27.48	16.16 ± 14.67	14.33 ± 13.79	13.46 ± 10.21	12.77 ± 23.43	8.64 ± 4.29
AF3	46.95 ± 27.52	16.62 ± 14.86	15.16 ± 15.46	16.93 ± 18.29	14.56 ± 27.49	7.46 ± 3.26

The typical traits of the IVIM parameters remain preserved in the accelerated sequences. However, D_t is systematically increased in accelerated sequences, whereas F_p is decreased.

*Statistical significance according to analysis of variance testing.

IVIM indicates intravoxel incoherent motion; *Dt*, diffusion coefficient; *Fp*, fraction of perfusion; D^*, pseudodiffusion coefficient; and AF, acceleration factor.

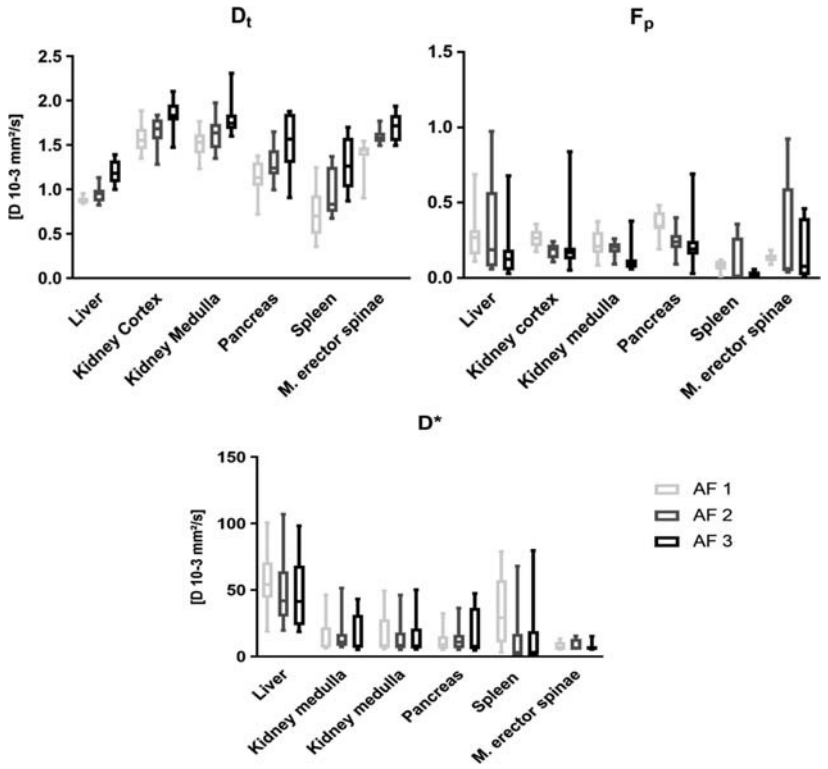

FIGURE 4. Whisker plot for D_t, F_p, and D^* showing similar tissue specific IVIM analysis results comparable to the literature.[23] D^* values remain highly varying.

consecutively forces the F_p to a lower value in the second IVIM calculation step. Second, the IVIM curve in SMS-DWI sequences partly loses the biexponential curve shape toward a more monoexponential behavior. This is supported by the IVIM measurements with the decreased F_p, which reflects the lower contribution of perfusion effects to the diffusion signal and causes the curve to follow a more monoexponential shape. The reason behind this finding might be that the antialiasing of the SMS-DWI sequences results in a smoothing of the b-value dependence of the signal curve. As acquisitions were performed without breath-holding, the antialiasing effect could be increased by breathing motion, which may cause fluctuations of the signal leakage in the slices across time,[24] thereby resulting in increased inaccuracy of the diffusion parameters. To further investigate this issue, another study may compare acquisitions with and without breath-holding. The leakage factor L, as proposed by Xu et al, may be applied to quantify the antialiasing effect due to the SMS technique. Nevertheless, if a moderate AF2 is applied, the curve shape does not significantly alter, for example, fast initial decay remains in liver and splenic tissue. A reduction of the TR due to slice acceleration could potentially introduce a T1 effect in the signal. However, we did not observe a dependence of calculated diffusion parameters on the T1 time of organs.

Our results are in line with previous publications. Intravoxel incoherent motion components D_t, F_p, and D^* are comparable to nonaccelerated IVIM values in the literature and show similar variations, for example, intermediate D_t and high D^* in liver parenchyma compared with the kidneys with higher D_t and much lower D^*.[25] In our study, the spleen shows a relatively high variability of computed parameters in the IVIM analysis. In the spleen, the strongly arterial perfusion with high blood velocity may cause high susceptibility to small positional displacements due to breathing motion. A first indication of a systematical deviation of SMS-DWI with higher acceleration factor was previously described in a feasibility study for pancreas and liver imaging.[21] In comparison to that previous report, our study included a higher number of subjects with more ROI measurements per organ, which may explain slight differences between mean IVIM parameters for the accelerated sequences. However, due to the higher number of

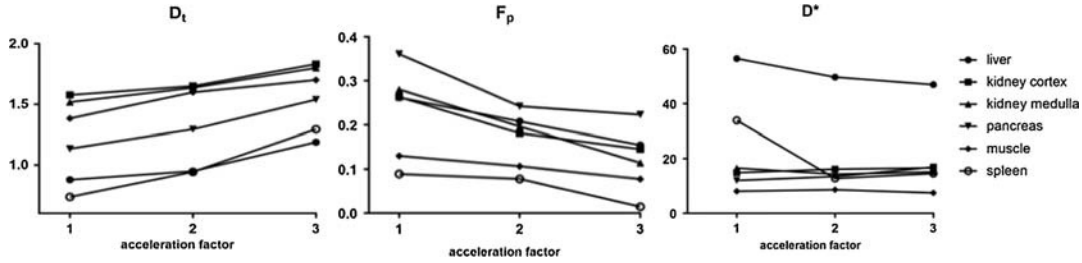

FIGURE 5. Behavior of the mean value of IVIM parameters D_t, F_p, and D^* for increasing acceleration factor AF1 to AF3. Note the significant increase ($P < 0.05$) of D_t and decrease of F_p with higher acceleration factor ($P < 0.05$) while there is no significant difference of D^* for different acceleration factors (eg, liver $P = 0.47$).

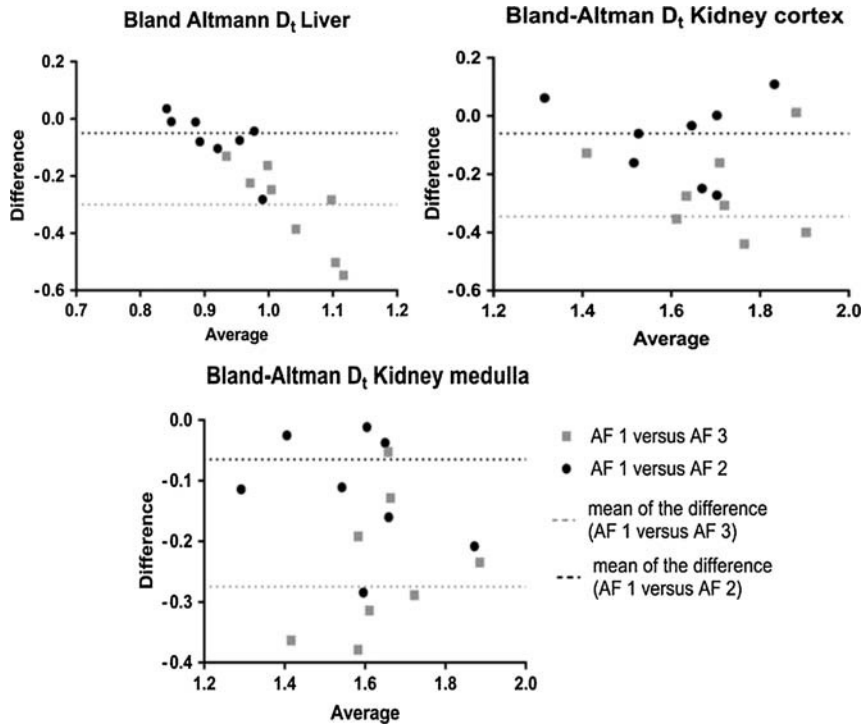

FIGURE 6. Bland-Altman plots for comparison of AF2 and AF3 with AF1 resulting in higher differences for AF3 toward AF1 than for AF2.

measurements, our parameter estimations may be regarded as more reliable. The same previous study found adequate diagnostic image quality and signal-to-noise ratio for high b-value DWI with SMS sequences in the liver and pancreas. Further studies from Filli et al[23] showed similar result regarding image quality in skeletal muscle imaging and breast[19] with optimal AF2 as a compromise between scan time reduction and image quality.

The study exhibits some limitations that need to be acknowledged. First, the study cohort is quite small. However, we found homogeneous results in the IVIM evaluations; therefore, the findings may be regarded as representative. Second, all volunteers were healthy volunteers, such that obtained conversion factors may probably not be directly applied to pathological tissue alterations. Also, because of the relatively lean young volunteers, we were not able to assess whether fat-saturation might constitute an obstacle in a patient cohort. Moreover, systematic deviations of pathological tissue were not evaluated, which was beyond the scope of this study. Here, further investigations are needed to find deviations of diffusion parameter with higher AF and compare it to the conversion factors of healthy tissue. Third, all measurements were performed in a 3 T MR scanner without comparison to lower field strength. However, as the technique of SMS acquisition is independent on the static field strength, similar results and trends can be expected in a 1.5 T magnetic field. In general, artifacts in DWI tend to increase in higher magnetic field due to higher susceptibility effects.

Intravoxel incoherent motion analysis in clinical examinations may provide many advantages compared with standard DWI due to the more thorough tissue characterization, for example, IVIM has been demonstrated to more accurately measure chemotherapy response of liver metastases or characterize hepatocellular carcinoma.[26] The additional acquisition of low b-values in the IVIM protocol results in prolonged TA of up to 15 minutes, which is incompatible with a clinical setting.[21] Applying SMS sequences, the TA can substantially be shortened, in our case, by 45% with an AF2 and 67% with an AF3. As slightly systematic deviations of IVIM parameters occur with increasing acceleration factor, the best compromise seems to be acceleration

TABLE 2. Conversion Table for IVIM Parameter D_t to Convert Between Different Acceleration Factors for All Upper Abdominal Organs

Liver	AF1	AF2	AF3	Renal Cortex	AF1	AF2	AF3	Renal Medulla	AF1	AF2	AF3
AF1	1	1.08	1.35	**AF1**	1	1.04	1.16	**AF1**	1	1.08	1.18
AF2	0.89	1	1.25	**AF2**	0.96	1	1.11	**AF2**	0.93	1	1.10
AF3	0.74	0.80	1	**AF3**	0.86	0.90	1	**AF3**	0.84	0.91	1
Pancreas	**AF1**	**AF2**	**AF3**	**Spleen**	**AF1**	**AF2**	**AF3**	**Erector Spinae Muscle**	**AF1**	**AF2**	**AF3**
AF1	1	1.14	1.35	**AF1**	1	2	1.74	**AF1**	1	1.16	1.23
AF2	0.88	1	1.18	**AF2**	0.5	1	1.37	**AF2**	0.86	1	1.06
AF3	0.74	0.84	1	**AF3**	0.36	0.73	1	**AF3**	0.81	0.94	1

IVIM indicates intravoxel incoherent motion; *Dt*, diffusion coefficient; and AF, acceleration factor.

TABLE 3. Conversion Table for IVIM Parameter F_p to Convert Between Different Acceleration Factors for All Upper Abdominal Organs

Liver	**AF1**	**AF2**	**AF3**	**Renal Cortex**	**AF1**	**AF2**	**AF3**	**Renal Medulla**	**AF1**	**AF2**	**AF3**
AF1	1	0.81	0.57	**AF1**	1	0.69	0.58	**AF1**	1	0.71	0.43
AF2	1.24	1	0.71	**AF2**	1.44	1	0.83	**AF2**	1.40	1	0.6
AF3	1.73	1.40	1	**AF3**	1.73	1.20	1	**AF3**	2.33	1.67	1
Pancreas	**AF1**	**AF2**	**AF3**	**Spleen**	**AF1**	**AF2**	**AF3**	**Erector Spinae Muscle**	**AF1**	**AF2**	**AF3**
AF1	1	0.67	0.61	**AF1**	1	0.88	0.11	**AF1**	1	0.85	0.62
AF2	1.5	1	0.92	**AF2**	1.13	1	0.125	**AF2**	1.18	1	0.73
AF3	1.64	1.10	1	**AF3**	9	8	1	**AF3**	1.62	1.38	1

IVIM indicates intravoxel incoherent motion; *Fp*, fraction of perfusion; and AF, acceleration factor.

with AF2 with scan time almost halved and nearly negligible deviation of the D_t and F_p values from the standard sequence. In the current study, we focused on the reduction of scan time. Further optimization aspects including number of averages and applied diffusion directions have not been addressed. In the current study, we focused on the reduction of scan time. Further optimization aspects including number of averages and applied diffusion directions have not been addressed. Future studies may include these optimizations, similar to the study of Kenkel et al,[22] to determine the best trade-off between image quality (eg, artifacts hampering diagnostic quality) and TA.

In conclusion, our study demonstrates that IVIM analysis based on SMS-DWI sequences is feasible resulting in a significant scan time reduction compared with standard sequences. A slight systematic deviation of the IVIM parameters D_t and F_p can be observed depending on the acceleration factor, which needs to be considered if measurements with different acceleration factors are compared. A conversion table to allow for comparison is provided in Table 2. According to our results, the best compromise between quantitation accuracy and reduction of scan time seems to be an AF2.

REFERENCES

1. Baliyan V, Das CJ, Sharma R, et al. Diffusion weighted imaging: technique and applications. *World J Radiol*. 2016;8:785–798.
2. Hagmann P, Jonasson L, Maeder P, et al. Understanding diffusion MR imaging techniques: from scalar diffusion-weighted imaging to diffusion tensor imaging and beyond. *Radiographics*. 2006;26 suppl 1:S205–S223.
3. Minematsu K, Li L, Fisher M, et al. Diffusion-weighted magnetic resonance imaging: rapid and quantitative detection of focal brain ischemia. *Neurology*. 1992; 42:235–240.
4. Donati OF, Chong D, Nanz D, et al. Diffusion-weighted MR imaging of upper abdominal organs: field strength and intervendor variability of apparent diffusion coefficients. *Radiology*. 2014;270:454–463.
5. Yu JS, Chung JJ, Kim JH, et al. Detection of small intrahepatic metastases of hepatocellular carcinomas using diffusion-weighted imaging: comparison with conventional dynamic MRI. *Magn Reson Imaging*. 2011;29:985–992.
6. Petralia G, Thoeny HC. DW-MRI of the urogenital tract: applications in oncology. *Cancer Imaging*. 2010;10(Spec no A):S112–S123.
7. Pozzi-Mucelli RM, Rinta-Kiikka I, Wünsche K, et al. Pancreatic MRI for the surveillance of cystic neoplasms: comparison of a short with a comprehensive imaging protocol. *Eur Radiol*. 2017;27:41–50.
8. Barth BK, Cornelius A, Nanz D, et al. Diffusion-weighted imaging of the prostate: image quality and geometric distortion of readout-segmented versus selective-excitation accelerated acquisitions. *Invest Radiol*. 2015;50:785–791.
9. Bakir B, Sanli S, Bakir VL, et al. Role of diffusion weighted MRI in the differential diagnosis of endometrial cancer, polyp, hyperplasia, and physiological thickening. *Clin Imaging*. 2017;41:86–94.
10. White NS, McDonald C, Farid N, et al. Diffusion-weighted imaging in cancer: physical foundations and applications of restriction spectrum imaging. *Cancer Res*. 2014;74:4638–4652.
11. Bonekamp S, Torbenson MS, Kamel IR. Diffusion-weighted magnetic resonance imaging for the staging of liver fibrosis. *J Clin Gastroenterol*. 2011;45:885–892.
12. Le Bihan D, Breton E, Lallemand D, et al. Separation of diffusion and perfusion in intravoxel incoherent motion MR imaging. *Radiology*. 1988;168:497–505.
13. Watanabe H, Kanematsu M, Goshima S, et al. Characterizing focal hepatic lesions by free-breathing intravoxel incoherent motion MRI at 3.0 T. *Acta Radiol*. 2014; 55:1166–1173.
14. Kakite S, Dyvorne HA, Lee KM, et al. Hepatocellular carcinoma: IVIM diffusion quantification for prediction of tumor necrosis compared to enhancement ratios. *Eur J Radiol Open*. 2015;3:1–7.
15. Guo Z, Zhang Q, Li X, et al. Intravoxel incoherent motion diffusion weighted MR imaging for monitoring the instantly therapeutic efficacy of radiofrequency ablation in rabbit VX2 tumors without evident links between conventional perfusion weighted images. *PLoS One*. 2015;10:e0127964.
16. Shirota N, Saito K, Sugimoto K, et al. Intravoxel incoherent motion MRI as a biomarker of sorafenib treatment for advanced hepatocellular carcinoma: a pilot study. *Cancer Imaging*. 2016;16:1.
17. Chilla GS, Tan CH, Xu C, et al. Diffusion weighted magnetic resonance imaging and its recent trend-a survey. *Quant Imaging Med Surg*. 2015;5:407–422.
18. Feinberg DA, Setsompop K. Ultra-fast MRI of the human brain with simultaneous multi-slice imaging. *J Magn Reson*. 2013;229:90–100.
19. Filli L, Ghafoor S, Kenkel D, et al. Simultaneous multi-slice readout-segmented echo planar imaging for accelerated diffusion-weighted imaging of the breast. *Eur J Radiol*. 2016;85:274–278.
20. Weiss J, Martirosian P, Taron J, et al. Feasibility of accelerated simultaneous multislice diffusion-weighted MRI of the prostate. *J Magn Reson Imaging*. 2017.
21. Boss A, Barth B, Filli L, et al. Simultaneous multi-slice echo planar diffusion weighted imaging of the liver and the pancreas: optimization of signal-to-noise ratio and acquisition time and application to intravoxel incoherent motion analysis. *Eur J Radiol*. 2016;85:1948–1955.
22. Kenkel D, Barth BK, Piccirelli M, et al. Simultaneous multislice diffusion-weighted imaging of the kidney: a systematic analysis of image quality. *Invest Radiol*. 2017;52:163–169.
23. Filli L, Piccirelli M, Kenkel D, et al. Simultaneous multislice echo planar imaging with blipped controlled aliasing in parallel imaging results in higher acceleration: a promising technique for accelerated diffusion tensor imaging of skeletal muscle. *Invest Radiol*. 2015;50:456–463.
24. Xu J, Moeller S, Auerbach EJ, et al. Evaluation of slice accelerations using multiband echo planar imaging at 3 T. *Neuroimage*. 2013;83:991–1001.
25. Wurnig MC, Donati OF, Ulbrich E, et al. Systematic analysis of the intravoxel incoherent motion threshold separating perfusion and diffusion effects: Proposal of a standardized algorithm. *Magn Reson Med*. 2015;74:1414–1422.
26. Granata V, Fusco R, Catalano O, et al. Intravoxel incoherent motion (IVIM) in diffusion-weighted imaging (DWI) for hepatocellular carcinoma: correlation with histologic grade. *Oncotarget*. 2016;7:79357–79364.